



**HAL**  
open science

## Parallel QR factorization of block-tridiagonal matrices

Alfredo Buttari, Søren Hauberg, Costy Kodsı

► **To cite this version:**

Alfredo Buttari, Søren Hauberg, Costy Kodsı. Parallel QR factorization of block-tridiagonal matrices. [Research Report] IRIT - Institut de recherche en informatique de Toulouse. 2019. hal-02370953v1

**HAL Id: hal-02370953**

**<https://hal.science/hal-02370953v1>**

Submitted on 19 Nov 2019 (v1), last revised 5 Nov 2020 (v2)

**HAL** is a multi-disciplinary open access archive for the deposit and dissemination of scientific research documents, whether they are published or not. The documents may come from teaching and research institutions in France or abroad, or from public or private research centers.

L'archive ouverte pluridisciplinaire **HAL**, est destinée au dépôt et à la diffusion de documents scientifiques de niveau recherche, publiés ou non, émanant des établissements d'enseignement et de recherche français ou étrangers, des laboratoires publics ou privés.

# Parallel $QR$ factorization of block-tridiagonal matrices

Alfredo Buttari<sup>1</sup>, Søren Hauberg<sup>2</sup>, and Costy Kodsı<sup>2</sup>

<sup>1</sup>Université de Toulouse, CNRS-IRIT

<sup>2</sup>DTU, Department of Applied Mathematics and Computer Science

2019-11-19

## Abstract

In this work, we deal with the  $QR$  factorization of block-tridiagonal matrices, where the blocks are dense and rectangular. This work is motivated by a novel method for computing geodesics over Riemannian manifolds. If blocks are reduced sequentially along the diagonal, only limited parallelism is available. We propose a matrix permutation approach based on the Nested Dissection method which improves parallelism at the cost of additional computations and storage. We provide a detailed analysis of the approach showing that this extra cost is bounded. Finally, we present an implementation for shared memory systems relying on task parallelism and the use of a runtime system. Experimental results support the conclusions of our analysis and show that the proposed approach leads to good performance and scalability.

## 1 Introduction

In this work, we deal with the solution of linear least squares problems where the system matrix is block-tridiagonal. By this we mean that our matrices have a block structure with  $c$  block-rows and  $c$  block-columns and along block-row  $k$  we only have nonzeros in block-columns  $k-1$  and  $k+1$  as depicted in Figure 1. The blocks are assumed to be dense and rectangular of size  $m \times n$  with  $m > n$ .

In a LAPACK-like  $QR$  factorization where sub-diagonal coefficients are eliminated by means of Householder reflections column-by-column in the natural order, only limited parallelism is available because of the lack of update operations (i.e., application of the Householder reflections to the trailing submatrix) stemming from the potentially narrow bandwidth and because each elimination step depends on the previous. Even the use of *tiled* [9] or *communication-avoiding* [12] approaches can barely improve the situation especially when  $c$  is high and  $m$  as well as  $n$  is small. By choosing a different order for reducing the

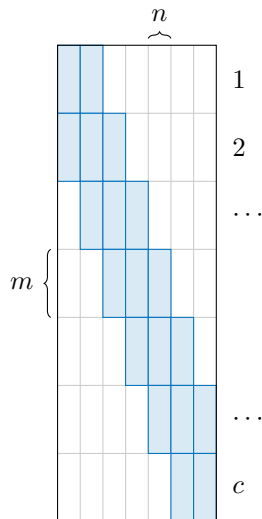


Figure 1: A block-tridiagonal matrix.

matrix columns, which essentially amounts to permuting the matrix columns, it is possible to achieve better parallelism; this, however, generates additional *fill-in* — coefficients that are zero in the original matrix and are turned into nonzeros by the factorization — which is responsible for an increase in the operation count and the storage. We propose an approach that computes this permutation by applying the Nested Dissection method to the compressed matrix graph. This allows us to identify groups of blocks that can be reduced independently; this first phase is followed by a reduction step that deals with the blocks that are at the interface of the groups. Although the structure and value of the  $R$  factor only depends on column permutations, the structure of the  $Q$  factor and, consequently, the overall cost of the factorization greatly depend on the order in which coefficients are annihilated within each column or, more generally, on row permutations. Taking this into account, we propose an approach that aims at reducing the operational complexity, especially in the reduction phase which involves communications. We provide a detailed analysis of the operational and memory cost showing that the overhead depends on how many nested dissection levels are used but is bounded by a modest constant. Finally, we present a parallel implementation for shared memory systems. This is based on the use of task parallelism where the whole workload is represented on the form of a *Directed Acyclic Graph* (DAG) of tasks which is automatically created and scheduled by a runtime system. This implementation is achieved using features of the `qr_mumps` software which rely on the StarPU runtime system. Experimental results obtained with this implementation shows that the proposed method achieves good performance and scalability on a 36 cores system and has the potential to perform even better on large-scale distributed

memory systems.

## 1.1 Motivation

One of the key challenges in *machine learning (ML)* is to learn (i.e., estimate) a representation of data that is suitable for a given task [5]. Learned representations for *supervised ML* tasks, such as classification and regression, are optimal only for specific tasks. In contrast, representations for *unsupervised ML* tasks, such as data exploration, are concerned with the underlying structure governing the observed data.

It has been shown in [16, 3] that an effective approach for unsupervised ML involves treating the learned representation as a *Riemannian manifold*. An unfortunate implication, however, is that vector space operations are no longer applicable. Instead, Riemannian counterparts, such as *logarithm* and *exponential maps* take the place of subtraction and addition operations. Also, *geodesics* in their role as generalizations of line segments in Euclidean space become prominent. Just as a segment of a line is the shortest distance connecting two distinct points, a geodesic on a Riemannian manifold is a smooth parametric curve that is a local length minimizer connecting any two distinct points. Additionally, a point moving along a geodesic does not experience acceleration in the tangent direction, i.e., the velocity has a constant magnitude.

Consider now an  $n$ -dimensional manifold embedded in  $m$ -dimensional Euclidean space (with  $m > n$ ) described by the parametric map

$$y : \mathbb{R}^n \rightarrow \mathbb{R}^m.$$

A rather simple and intuitive strategy for determining a geodesic given any two distinct points on a Riemannian manifold requires working with the discretized version of a smooth parametric curve. It is then possible to model the curve as a *series of connected linear elastic springs*. A spring force  $f \in \mathbb{R}^m$  is related to the end points  $y(x_i), y(x_j) \in \mathbb{R}^m$  of a curve segment by  $f = K(y(x_j) - y(x_i))$ , in which  $x \in \mathbb{R}^n$  and  $K$  is the identity matrix representing the stiffness. Even though the springs are linear in nature, the parameterization introduces potential nonlinearity. Imposing boundary conditions (constituting the given points) on the assembled block tridiagonal (total) stiffness matrix as well as force vector, a system of equations can be solved for the unknown curve points yielding the stable equilibrium of the spring assemblage and geodesic. If a system of nonlinear equations has to be tackled, which is the working assumption, Newton's method or a variation of Newton's method is a popular choice. In each iteration of Newton's method, the solution of an overdetermined system of linear equations featuring a full-rank Jacobian is sought as a trial step. *QR* factorization of the Jacobian is very much desirable as the conditioning of the problem is not subject to unnecessary degradation.

## 1.2 Related work

Our work can be related to the factorization of banded, (block) bi or tridiagonal matrices. Most of the approaches presented in the literature draw parallelism from *cyclic reduction* [19], *wrap-around* [17], partitioning methods or minor variants thereof; these techniques amount to identifying independent sets of computations that allow for reducing multiple (block) columns at once at the cost of additional computations due to fill-in. The method we propose in this work relies on the use of nested dissection (see Sections 2.1 and 2.2) and, essentially, leads to permutations that are equivalent to those computed with cyclic reduction or wrap-around; because nested dissection relies on graph theory, we believe it provides a clearer framework that allows for a better understanding and analysis of parallelism and fill-in.

Early work on the  $QR$  factorization of square tridiagonal systems by Givens rotations is proposed by Sameh and Kuck [24]. Computations are organized in two stages. In the first diagonal blocks are reduced independently; this introduces fill-in at the interface of contiguous diagonal blocks which is reduced in the second stage. These ideas eventually lead to the definition of *spike* [23, 21] algorithm for the  $LU$  factorization of banded matrices. This approach was also used by Berry and Sameh [6] to compute the parallel  $LU$  factorization of block-tridiagonal, diagonally dominant (i.e., they do not require pivoting) matrices.

Arbenz and Hegland [2] propose a method for the stable solution of (periodic) square banded linear systems. The factorization is achieved in two phases assuming that the original matrix is permuted into *standard form* (i.e., lower-banded periodic) through a circular shift; this permutation introduces some unnecessary fill-in. In the first phase, a partitioning of the matrix (which amounts to a dissection step) and block-columns associated with the resulting parts are reduced independently. This leads to a periodic block-bidiagonal system which is reduced in parallel using cyclic reduction. They discuss both the  $LU$  and  $QR$  factorization although mostly focus on the first. Note that the  $QR$  factorization of square, periodic block-bidiagonal systems through cyclic reduction is also addressed by Hegland and Osborne [18]

None of the aforementioned approaches consider the case of overdetermined systems; this has non-trivial implications because when a block-column is reduced, some coefficients along the corresponding pivotal block-row remain which have to be reduced. Also, all of these methods only draw parallelism from the matrix permutation or partitioning whereas our approach exploits multiple levels of parallelism as described in Section 3.

All of the methods referenced, including ours, are, in essence, specialized multifrontal methods [13]. Algebraic multifrontal methods for the  $QR$  factorization of sparse matrices have been proposed in the literature by Amestoy, Duff, and Puglisi [1], Davis [11] and Buttari [8], for instance. These methods and the corresponding tools are designed for generic sparse matrices; although they can obviously be used for solving block-tridiagonal systems, they may not be the best suited tools. Indeed, unlike common sparse matrices, our block-tridiagonal

systems may be relatively dense in the beginning (multiple thousands of coefficients per row) and fill up moderately during the factorization (see Section 2.4). As a result, algebraic sparse multifrontal solvers may suffer from the excessive overhead due to the handling of the coefficients of the original matrix based on indirect addressing. Clearly, these methods could be extended to efficiently handle block matrices; this is the object of future work. Additionally, multifrontal methods involve explicit assembly of frontal matrices which can be avoided in our case due to the simple, regular structure of the data (see Section 2.3). Finally, in sparse multifrontal solvers, frontal matrices are typically reduced using a LAPACK-like factorization which does not fully take into account their possibly sparse nature as explained in Section 2.3.

## 2 Algorithm

In this section we describe our approach to parallelize the  $QR$  factorization of a block-tridiagonal matrix. Our description and analysis will rely on the theory of sparse matrix factorizations. The necessary theoretical background is briefly described in the next section; we refer the reader to the cited documents for a detailed discussion of this topic.

### 2.1 Preliminaries

As it is commonly done in the literature [10, 8], our symbolic analysis of the  $QR$  factorization of a sparse matrix relies on the equivalence between the  $R$  factor of a real matrix  $A$  and the Cholesky factor of the normal equations  $B = A^T A$ . As a result of this equivalence, the  $QR$  factorization of a sparse matrix  $A$  follows the same computational pattern as the Cholesky factorization of  $B$ . This can be modeled using the *adjacency graph* of  $B$  defined as a graph  $\mathcal{G}(B) = (\mathcal{V}, \mathcal{E})$  whose vertex set  $\mathcal{V} = \{1, 2, \dots, cn\}$  includes the unknowns of  $B$  and edge set  $\mathcal{E} = \{(i, j) \mid b_{i,j} \neq 0\}$  includes an edge for each nonzero coefficient of  $B$ . In our case, the symmetry of  $B$  implies that if  $(i, j)$  is in  $\mathcal{E}$ , then so is  $(j, i)$ , and therefore we will only represent one of these edges; such a graph is called *undirected*.

It is possible to use the adjacency graph to model the Cholesky factorization of  $B$ . Specifically we can build a sequence of graphs  $\mathcal{G}(B) = \mathcal{G}_0(B), \mathcal{G}_1(B), \dots, \mathcal{G}_{cn-1}(B)$ , called *elimination graphs*, such that  $\mathcal{G}_k(B)$  is the adjacency graph of the trailing submatrix after elimination of variables  $1, 2, \dots, k$ . Elimination graph  $\mathcal{G}_k(B)$  is built from  $\mathcal{G}_{k-1}(B)$  by removing node  $k$  as well as all its incident edges and by updating the connectivity of the remaining nodes: for any two nodes  $i$  and  $j$  that are neighbors of  $k$ , we have to add an edge connecting them if it does not exist already. One such edge, called a *fill edge*, models the occurrence of a new *fill-in* coefficient.

A sparse factorization can achieve better parallelism than a dense one because sparsity implies that the elimination of one unknown does not affect all the uneliminated ones but only part of them. The dependencies between variables are represented by the so-called *directed filled graph* which corresponds to

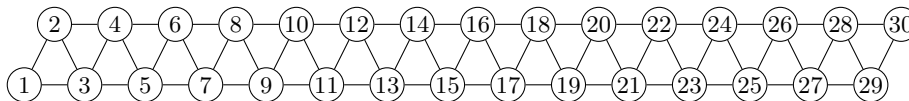


Figure 2: Compressed graph for the normal equations  $B = A^T A$ . The label inside nodes show the unknown number which, in this case, corresponds to the order in which unknowns are eliminated.

the original graph  $\mathcal{G}(B)$  plus all the fill edges; in this graph an edge  $(i, j)$  is directed from  $i$  to  $j$  if  $j$  is eliminated after  $i$  and expresses the fact that  $j$  depends on  $i$ . Because many of the dependencies expressed by the filled graph are redundant, its transitive reduction is computed to obtain the smallest complete set of dependencies; this results in a tree graph called an *elimination tree*. The elimination tree plays a central role in sparse matrix factorizations [20] because it dictates the order in which the unknowns can be eliminated: any order that follows a topological (i.e., bottom-up) traversal of the tree leads to the same result. A consequence of this fact is that nodes belonging to different branches are independent and can, thus, be eliminated in parallel. Nodes of the elimination tree are commonly amalgamated into supernodes containing nodes that share the same neighbors in the filled graph and can thus be eliminated at once; the resulting amalgamated tree is commonly referred to as an *assembly tree*.

*Nested Dissection* is a method introduced by George [15] to reduce the complexity of sparse factorizations. The basic step of this method is based on the idea of computing a separator  $\mathcal{S}$  of a graph  $\mathcal{G}$ ; this is defined as a subset of nodes which splits the graph into two non-connected subgraphs  $\mathcal{G}_1$  and  $\mathcal{G}_2$ . If the nodes in  $\mathcal{S}$  are eliminated last, no fill-in is possible between the nodes of  $\mathcal{G}_1$  and those of  $\mathcal{G}_2$  because of the Rose, Tarjan and Lueker theorem [22]. This generally reduces the overall amount of fill-in and improves parallelism because the nodes of  $\mathcal{G}_1$  can be eliminated independently, and, thus in parallel, than those of  $\mathcal{G}_2$ . Nested Dissection applies this procedure recursively until subgraphs of a given minimum size are achieved. The resulting tree of separators matches the assembly tree.

## 2.2 A Nested Dissection based approach

Because our matrices are made of dense blocks, our analysis can focus on the *compressed graph* where a node represents all the unknowns in a block-column and an edge represents a set of edges that connect all the unknowns in one block-column to all those in another block-column. Figure 2 shows the compressed graph for the normal equations  $B = A^T A$ ; this can be easily derived knowing that  $b_{i,j} \neq 0$  if there exist a row  $k$  in  $A$  such that  $a_{k,i} \neq 0$  and  $a_{k,j} \neq 0$ . Because all the columns (rows) within a block-column (block-row) are indistinguishable, we will use the term “column” (“row”) to refer to a block-column (block-row).

A few observations can be made about this graph. First, regardless of the order in which unknowns are eliminated, some fill-in will appear in  $R$ . In fact, although block-row  $k$  of  $A$  only has nonzero blocks in block-columns  $k - 1$  and  $k + 1$ ,  $R$  will also have a nonzero block in block-column  $k + 2$ ; these fill-in blocks are represented by the horizontal edges in Figure 2. Second, if unknowns are eliminated in the natural order, no additional fill-in is introduced in  $R$  by the factorization. This is because, upon elimination of node  $k$ , its neighbors are already connected to each other. Third, the transitive reduction of the graph in Figure 2 leads to a linear graph, i.e., a tree with a single branch which does not provide any opportunities for parallelism.

Nested dissection can be used to improve parallelism as briefly explained in the previous section. One level of dissection can be applied by choosing, for example, the two middle nodes as a separator as shown in the top graph of Figure 3, where the nodes have been re-labeled to match the elimination order. This leads to the tree shown in the bottom left part of the same figure. This tree has two separate branches which can be traversed in parallel. It must be noted that the order in which the nodes on the right of the separator are visited is reversed with respect to the original one; as a result, in this case, no additional fill-in is added because the nodes are eliminated starting at both ends of the graph.

Additional parallelism can be achieved by recursively applying this bisection step. Figure 3 shows two levels of nested dissection lead to a tree with four parallel branches. It must be noted, though, that in this case some fill-in is generated when processing the nodes in the two middle branches; for example, upon elimination of node 7, three fill edges appear to connect nodes 8, 9, 29 and 30 to each other, as described in the elimination graph procedure presented in the previous section. With additional levels of nested dissection, a moderate increase in the fill-in happens as a result of more nodes being processed in internal branches rather than the two outer ones; this will be quantified shortly.

The nested dissection method is commonly used for reducing the complexity of a sparse factorization. In our case, although it is very effective in improving parallelism, it increases the overall cost of the factorization both in terms of flop count and memory consumption. Consequently, operations have to be scheduled carefully to keep this overhead as low as possible and a model of the factorization complexity as a function of the number of nested dissection levels  $l$  must be computed to understand whether a suitable compromise between these two parameters can be found. This is the objective of the next section.

### 2.3 Node elimination

Our  $QR$  factorization algorithm can be roughly described as a method which runs in  $c$  steps,  $c$  being the number of block-columns, where at step  $k$  all the nonzero blocks in column  $k$  are annihilated except one which is, instead, reduced to a triangle; as a result of this column reduction we obtain one block-row of the



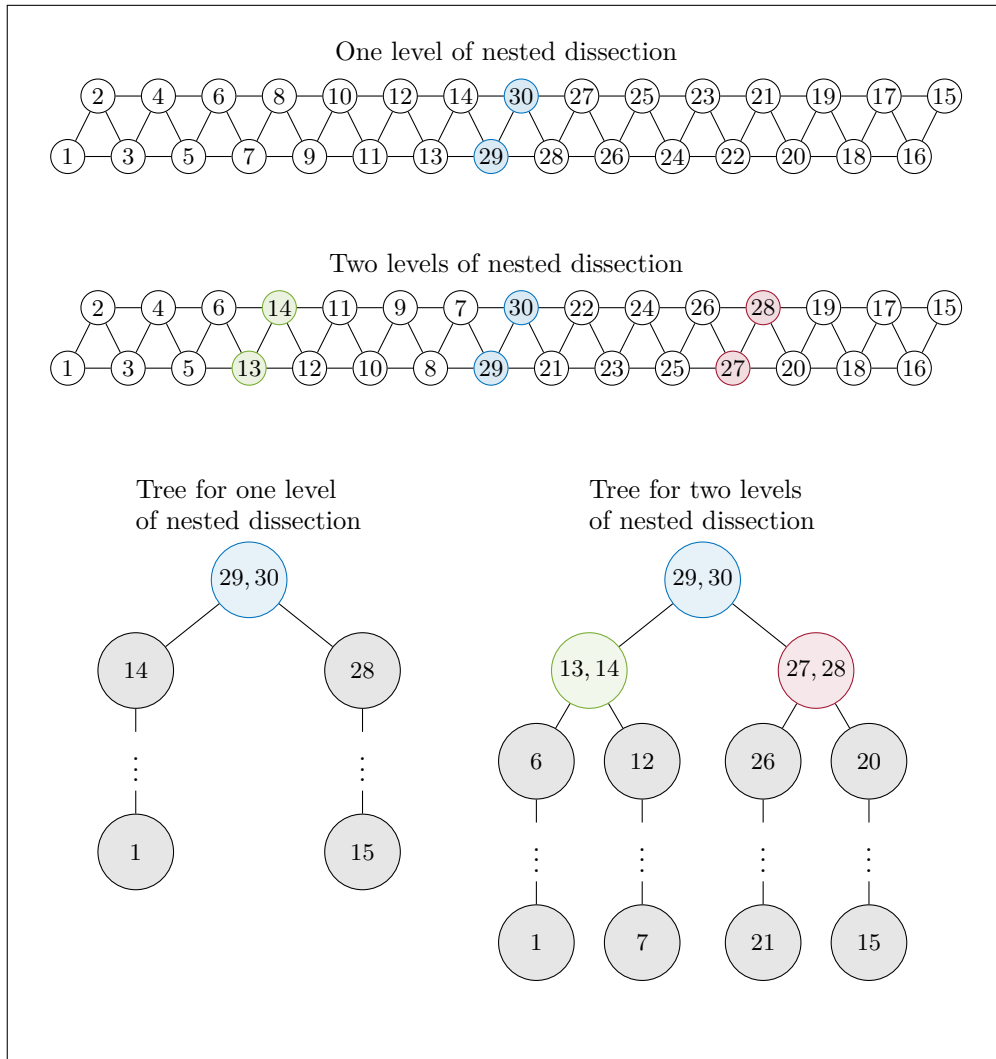


Figure 3: The effect of one and two levels of nested dissection on the compressed graph of the normal equations.

global  $R$  factor. The annihilation of a block not only involves its block-row but also a second one which we refer to as *pivotal row*; if, for example, the blocks are of size  $1 \times 1$ , this can be achieved by a Givens rotation. In our case, because we are dealing with dense blocks of potentially large size, Householder reflections will be used instead because they heavily rely on Level-3 BLAS operations and, therefore, can achieve much higher performance on modern processors; the LAPACK library provides the basic operations to achieve these transformations which are presented below. As a result of a block annihilation in column  $k$ ,

the structure of both the involved rows in columns  $k + 1, \dots, c$  will be equal to the union of their prior structures. This implies that some fill-in may be introduced by the transformation; additionally this fill-in depends on which pivotal row is chosen to annihilate a block. It must be noted that different pivotal sequences always lead to the same (numerically)  $R$  factor which only depends on column permutations; as a consequence, different pivotal sequences only have an effect on the  $Q$  factor. Several strategies were proposed in the past for choosing pivotal sequences that reduce the fill-in; the approach that we adopted in our work relates to the *variable pivoting* technique proposed by Gentleman [14] for the  $QR$  factorization of sparse matrices by means of Givens rotations; this can be summed up as a method where, when an entry in position  $(i, k)$  has to be annihilated, a pivotal row  $j$  is chosen such that its structure is as close as possible to that of row  $i$ .

Our algorithm can be implemented using the `geqrt`, `gemqrt`, `tpqrt` and `tpmqrt` elementary operations which are available in the LAPACK library. The first of these, `geqrt`, computes the  $QR$  factorization of a rectangular block; the second, `gemqrt`, updates a block by applying the  $Q$  matrix (or its transpose) resulting from a `geqrt` operation; the third, `tpqrt`, computes the  $QR$  factorization of a matrix formed by a triangular block on top of a pentagonal one (in our case it will only be either rectangular or triangular); the fourth, `tpmqrt`, updates a couple of blocks by applying the  $Q$  matrix (or its transpose) resulting from a `tpqrt` operation. Without loss of generality, we assume that the number of rows in a block is at least twice the number of columns, i.e.,  $m \geq 2n$ ; therefore, each block can be logically split into three parts with the third being, possibly, empty: the first containing rows  $1, \dots, n$ , the second containing rows  $n + 1, \dots, 2n$  and the third containing rows  $2n + 1, \dots, m$ . We will refer to these parts using a bitmap: for example  $A^3$  denotes the first and second parts of a block  $A$ . The algorithm will be described using the following notation:

- $GE(B_{i,j}^u)$ : corresponds to reducing part  $u$  of the block in row  $i$  and column  $j$  through a `geqrt` operation and updating all the corresponding blocks in row  $i$  using `gemqrt` operations;
- $TP(B_{i,j}^u, B_{k,j}^v)$ : corresponds to annihilating part  $v$  of the block in position  $(k, j)$  using part  $u$  of the block in position  $(i, j)$  through a `tpqrt` operation and updating the corresponding blocks along rows  $i$  and  $k$  with `tpmqrt` operations.

An example of the use of this notation is provided in Figure 4.

At each node of the tree, one column of the matrix is reduced (two for nodes associated with separators). The nodes of the tree can be classified into four different types: leaf, chain, separator and root nodes. The first corresponds to the nodes that are at the lowest level of the tree (e.g., nodes 7 or 15 in the bottom-right tree of Figure 3); the second corresponds to nodes in the sequential branches associated with the subdomains resulting from nested dissection (e.g., node 12 or 20 in Figure 3); the third corresponds to nodes belonging to some separator (e.g., node (13, 14) in Figure 3); the fourth is the root node of the

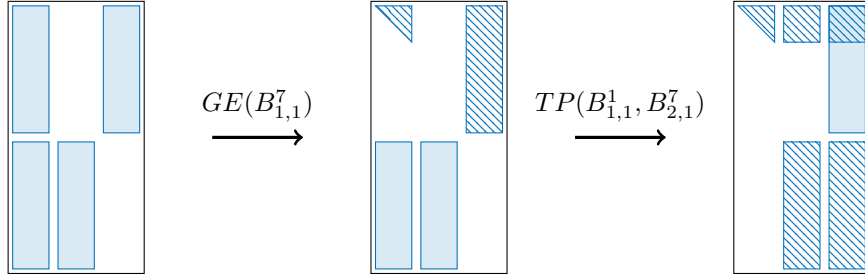


Figure 4: Example showing the use of the notation used to describe pivotal sequences. The data modified at each step are shown with a fill pattern.

tree. For each type, a different pivotal sequence is used; moreover, for each type, nodes belonging to the two outer branches need some special treatment, as explained below. For the sake of readability, here we only provide the pivotal sequence for a chain node because this is where most of the computations are done assuming  $c \gg 2^l$ ; the other node types are discussed in the appendix.

Reducing a column  $k$  associated with one of these nodes affects blocks in columns  $k$ ,  $k + 1$ ,  $k + 2$  and columns  $a_1$  and  $a_2$  associated with the separator that the chain is moving away from and rows  $k + 1$  and  $a_1$ . For example, when node 8 in Figure 3 (*bottom-right*) is visited, it is connected to nodes 9, 10, 29 and 30 (because node 7 has been previously eliminated) which explains why these columns are concerned by its elimination. Note also that when node  $k$  is visited, block-rows  $k$  and  $a_1$  and block-columns  $k$ ,  $k + 1$ ,  $a_1$  and  $a_2$  have been already updated upon processing of nodes that are lower in the same branch; this leads to the particular structure which is illustrated in the left part of Figure 5. The pivotal sequence that we use on chain node  $k$  is:

$$\begin{aligned}
 &GE(B_{k+1,k}^7), \quad TP(B_{k,k}^1, B_{k+1,k}^1), \quad GE(B_{k+1,k+1}^7), \\
 &TP(B_{k+1,k+1}^1, B_{k,k+1}^2), \quad GE(B_{k+1,k+2}^6), \quad TP(B_{k+1,k+2}^2, B_{k,k+2}^2), \\
 &TP(B_{a_1,a_1}^1, B_{k,a_1}^2), \quad TP(B_{a_1,a_1}^1, B_{k+1,a_1}^4), \\
 &TP(B_{a_1,a_2}^2, B_{k,a_2}^2), \quad TP(B_{a_1,a_2}^2, B_{k+1,a_2}^4).
 \end{aligned}$$

These operations transform the blocks shown in the left part of Figure 5 into those shown in the right part of the same figure. After these transformations, the blocks in row  $k$  (highlighted in red in the figure) are in their final state and will not be updated anymore; the blocks in rows  $k + 1$  and  $a_1$  will, instead, be updated in the parent node. Finally, the blocks that are grayed out end up in the  $H$  matrix that implicitly represents  $Q$  by means of the Householder vectors; these are also in their final state will not be modified anymore. This process closely resembles the  $QR$  multifrontal method [1, 11, 8] where the structure that gathers all the coefficients concerned by the reduction of one column is called a *multifrontal matrix*. It must be noted, however, that in the multifrontal method,

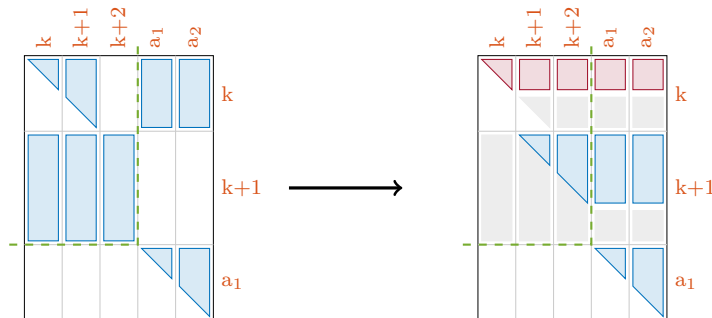


Figure 5: The blocks concerned by the operations at chain node  $k$ . Their structure before and after the processing of the node are shown in the left and right parts of the figure, respectively. The green dashed line shows the difference between inner and outer chain nodes.

frontal matrices are explicitly assembled by copying coefficients into a dense matrix data structure; these copies can be extremely costly due to the large size of blocks. Additionally, the multifrontal method can only take advantage of the zeroes in the bottom-left part of frontal matrices (this is referred to as “Strategy 3” in the work of Amestoy, Duff, and Puglisi [1]) whereas, through the use of variable pivoting, our approach can avoid more unnecessary computations. Note that the two outer chains advance from one end of the graph towards the center and, therefore, they do not move away from any separator. As a result only columns  $k$ ,  $k + 1$  and  $k + 2$  and rows  $k$  and  $k + 1$  are concerned by the elimination of the nodes therein; this is illustrated with a green dashed line in Figure 5. Consequently, the last four operations in the pivotal sequence above need not be executed on these nodes.

## 2.4 Complexity

The cost of the elementary operations that are used in our method are reported in Table 1. For the `tpqrt` and `tpmqrt` operations, two cases are reported: the first (in the middle column) where the bottom block is a rectangle of size  $p \times n$  and the second (in the right column) where the bottom block is a triangle of size  $n \times n$ . Note that,  $p$  is a generic block-row size and, in the algorithm of the previous section, it does not necessarily correspond to the row size  $m$  of an entire block but the part that is actually concerned by the operation. The number of columns, instead, will always be equal to  $n$  (the block column size) which is assumed to be the same for all blocks.

Summing up the values in Table 1 for the operations of the pivotal sequence from the previous section yields the value in row two, column three of Table 2. For a node in an outer chain, the cost, reported in row and column two, is lower because fewer operations are needed as explained in the previous section. In the top rows of the table we also report the operational complexity of all the other

geqrt	$2n^2(p - n/3)$	tpqrt	$2pn^2$	tpqrt*	$2n^3/3$
gemrt	$2n^2(2p - n)$	tpmqrt	$4pn^2$	tpmqrt*	$2n^3$

Table 1: Operational complexity of the elementary operations.  $p$  corresponds to the number of rows in a block that are concerned by the operation.

	Outer	Middle
Leaf	$\mathcal{F}_{lo} = 32mn^2 - 16n^3$	$\mathcal{F}_{lm} = 86mn^2 - 100n^3/3$
Chain	$\mathcal{F}_{co} = 18mn^2 - 2n^3/3$	$\mathcal{F}_{cm} = 42mn^2 - 2n^3/3$
Separator	$\mathcal{F}_{so} = 34mn^2 - 10n^3/3$	$\mathcal{F}_{sm} = 98mn^3 - 10n^3/3$
Root	$\mathcal{F}_{ro} = 8mn^2$	$\mathcal{F}_{rm} = 16n^3/3$
Leaf	$\mathcal{M}_{lo} = mn + 5mn$	$\mathcal{M}_{lm} = 4mn + 2n^2 + 9mn$
Chain	$\mathcal{M}_{co} = 2n^2 + 3mn$	$\mathcal{M}_{cm} = 2mn + 2n^2 + 3mn$
Separator	$\mathcal{M}_{so} = 3n^2$	$\mathcal{M}_{sm} = 12n^2$
Root	$\mathcal{M}_{ro} = 2mn$	$\mathcal{M}_{rm} = 0$

Table 2: Flops (*top*) and storage (*bottom*) count at each node of the tree. Each value in the top part is computed as a sum of the complexity of the elementary operations reported in Table 1 over the corresponding pivotal sequence. Each value in the bottom part is computed as the difference between the structure of blocks before and after processing the corresponding node.

node types and we refer the reader to the appendix for details of the related pivotal sequences. With a slight abuse of notation, we denote “outer root” the root of the tree for the case  $l = 0$  and “middle root” the tree root for the case  $l > 0$ .

By the same token, it is possible to compute the amount of memory (in number of coefficients) consumed at each node type, reported in the bottom part of Table 2; this is made of the blocks coming from the original matrix (highlighted in red in the table) plus the fill-in generated during the processing of the node (for example, for chain nodes this can be computed as the difference between the right and left parts of Figure 5).

Summing up the values in Table 2 for all the nodes of the tree leads to the overall cost of the factorization, which is

$$\begin{aligned}
\mathcal{C}(c, l > 0) &= (2^l - 2)\mathcal{C}_{lm} + 2\mathcal{C}_{lo} && \% \text{ leaf nodes} \\
&+ (2^l - 2) \left(\frac{c+2}{2^l} - 3\right) \mathcal{C}_{cm} + 2 \left(\frac{c+2}{2^l} - 3\right) \mathcal{C}_{co} && \% \text{ chain nodes} \\
&+ (2^l - 2 - 2(l-1)) \mathcal{C}_{sm} + 2(l-1)\mathcal{C}_{so} && \% \text{ separator nodes} \\
&+ \mathcal{C}_{rm} && \% \text{ root node} \\
\\
\mathcal{C}(c, l = 0) &= \mathcal{C}_{lo} && \% \text{ leaf nodes} \\
&+ (c-3)\mathcal{C}_{co} && \% \text{ chain nodes} \\
&+ \mathcal{C}_{ro}. && \% \text{ root node}
\end{aligned} \tag{1}$$

In the above formula,  $\mathcal{C}$  can be replaced with either  $\mathcal{F}$  or  $\mathcal{M}$  leading to, respectively, the overall flop count or the overall memory consumption.

In this formula, for the case where no nested dissection is used (i.e.,  $l = 0$ ), the root node corresponds to the penultimate chain node where the last two block-columns of the matrix are reduced.

Figure 6 shows how the relative cost of the factorization, respectively  $\mathcal{F}(c, l)/\mathcal{F}(c, 0)$  and  $\mathcal{M}(c, l)/\mathcal{M}(c, 0)$ , varies for different problem sizes and different levels of nested dissection for the case where  $m = 2n$ ; it is possible to see that, for growing values of  $l$  and  $c$ , these curves converge to, respectively,  $\mathcal{F}_{cm}/\mathcal{F}_{co}$  and  $\mathcal{M}_{cm}/\mathcal{M}_{co}$  because for  $l = 0$  the tree is essentially made of a single outer chain, whereas for large  $l$  and  $c$  values the vast majority of computations are done in nodes belonging to middle chains. For growing values of  $m$ , these two ratios converge, respectively, to  $2.3\bar{3}$  and  $1.6\bar{6}$ .

Other pivotal sequences can be used on each node type. Finding an optimal pivotal sequence is an extremely challenging task due to its combinatorial nature. The sequence(s) proposed above, however aim at achieving as many operations as possible within the chains which can be processed in an embarrassingly parallel fashion; indeed all the operations in separator nodes only involve parts of blocks that are of size  $n \times n$  (either square or triangular; see the appendix for further details). This is likely to reduce the relative weight of the reduction phase associated with the top part of the tree where communications happen.

### 3 A solver with multiple levels of parallelism

In this section, we describe how an actual parallel implementation of the described algorithm was achieved. However, we only address a version for shared memory systems (e.g., single node, multicore machines).

As explained, our method relies on four basic kernels which are used to achieve the pivotal sequences described in Section 2.3 and in the appendix. Although these kernels are available in the LAPACK library, we have chosen to rely on their implementation in the `qr_mumps` library. This software implements a sparse multifrontal solver based on the  $QR$  factorization; as such it relies on dense linear algebra operations for processing frontal matrices. Among others, `qr_mumps` provides an implementation of the `geqrt`, `gemqrt` operations; to these

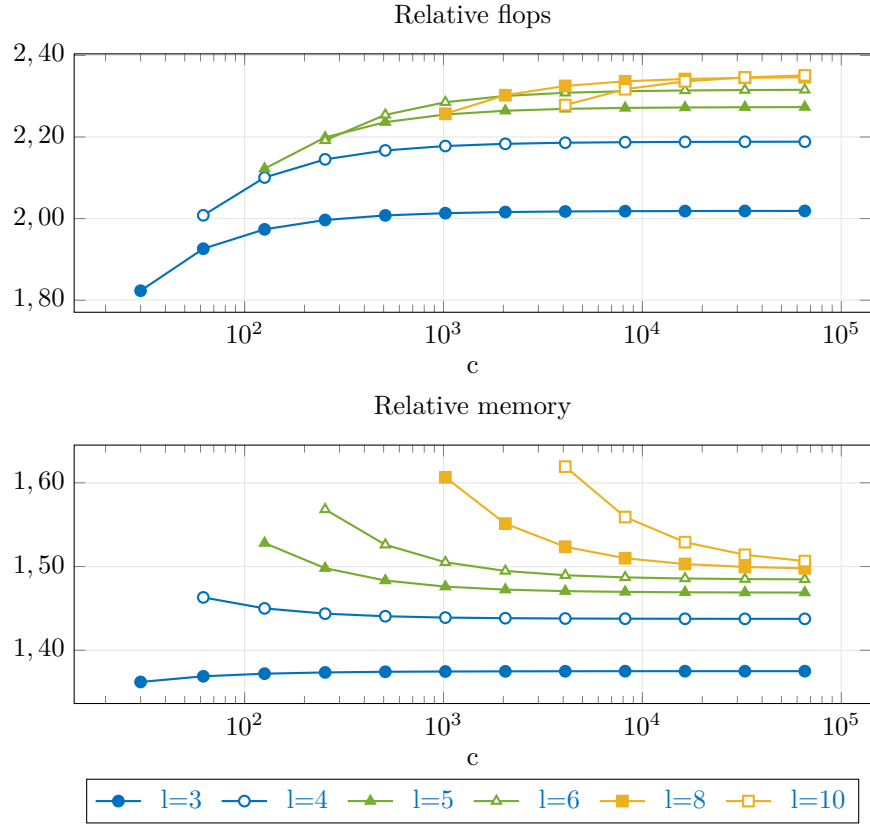


Figure 6: Relative number of floating point operations (*top*) and memory consumption (*bottom*) with respect to the case where no nested dissection based permutation is used for the case  $m = 2n$ .

we have added an implementation of the `tpqrt` and `tpmqrt` ones (see below for the details).

One immediate advantage of this choice is that, in `qr_mumps` these operations are efficiently parallelized. As a result some parallelism can be achieved within each node of the tree and, thus, even in the case where no nested dissection permutation is used. The parallelization of these operations relies on *tiled* algorithms [9] (also referred to as *communication avoiding*): blocks are divided into square tiles of size  $b \times b$  which are eliminated by means of block Householder transformations according to different schemes [7] which aim at improving concurrency by reducing unnecessary synchronizations and communications. Our implementation of the `tpqrt` and `tpmqrt` operations relies on the same approach and uses a tile elimination scheme which is referred to as Sameh-Kuck by Bouwmeester et al. [7]: the tiles in the trapezoidal block (remember that we only consider the two special cases where the trapezoidal degenerates

to a triangle or a rectangle) along a column are eliminated one after the other starting from the top using the corresponding diagonal tile in the triangular block.

`qr_mumps` relies on task based parallelism for the implementation of these methods. The workload is represented in the form of a Directed Acyclic Graph (DAG) where nodes are elementary operations (e.g., elimination of a tile) and edges are the dependencies among them; this representation allows for very quick access to all the available concurrency at any moment during the execution and for using very dynamic and asynchronous execution approaches. `qr_mumps` achieves task based parallelism through the use of a *runtime system*, namely StarPU [4], which provides a programming interface for defining the DAG and a scheduling engine for tracking the status of the DAG and triggering the execution of ready tasks on the available processing units. StarPU provides a programming API based on the Sequential Task Flow (STF) model (sometimes also referred to as *superscalar*). In this model, a master thread submits tasks to the runtime specifying how each of them accesses the data (whether in read or write mode); based on this information and the tasks submission order, the runtime can automatically define the dependencies among tasks and generate the DAG. This model is also used in the OpenMP standard (through the `task` directive and the `depend` clause) and other runtime systems.

Additional parallelism besides that available among different branches of the tree and within each block operation is achieved through the use of `qr_mumps` asynchronous API. With the standard synchronous API, each call to an operation is blocking, which means that control is returned to the caller only after the DAG for that operation is created and all of its tasks are executed. With the asynchronous API, instead, only the DAG is created and control is immediately returned to the caller; methods are available in `qr_mumps` to check whether all the tasks associated with one called operation have been executed. When multiple operations have to be executed, asynchronous calls can be made for all of them, which will generate a single DAG for all at once where dependencies are inferred between tasks belonging to different operations that access the same data. Thanks to the availability of this asynchronous interface, our implementation of the block tridiagonal  $QR$  factorization algorithm described in the previous section consists of a sequential code that traverses the tree in a topological order and, for each node, calls the `qr_mumps` operations corresponding to the pivotal sequences described and in the appendix; parallelism is automatically taken care of by `qr_mumps`.

## 4 Experimental results

In this section we report experimental results that illustrate the behavior of the algorithm presented in Section 2 and its implementation described in Section 3. These were obtained on one node of the Olympe supercomputer of the CALMIP regional supercomputing center in Toulouse, France. One such node is equipped with two Intel(R) Xeon(R) Gold 6140 CPUs for a total of 36 cores. We have



		$l$					
		0	1	2	3	4	5
#threads	1	153.8	-	-	-	-	-
	2	78.9	77.7	-	-	-	-
	4	40.4	39.0	57.9	-	-	-
	8	26.3	20.2	29.7	34.8	-	-
	16	25.8	15.2	17.0	19.7	21.3	-
	32	25.9	15.6	12.5	14.5	15.3	16.1
	36	26.5	17.3	14.5	15.1	16.0	16.4
#threads	1	149.1	-	-	-	-	-
	2	81.9	74.2	-	-	-	-
	4	59.4	40.7	55.9	-	-	-
	8	52.5	29.8	27.5	32.6	-	-
	16	53.2	28.7	16.7	18.0	19.3	-
	32	57.3	28.7	15.3	9.7	10.1	10.7
	36	67.1	34.7	15.9	9.6	9.4	9.7

Table 3: Execution time for the  $QR$  factorization of a problem with  $m = 640$ ,  $n = 320$  and  $c = 4094$  with tile size  $b = 160$  (*top*) and  $b = 320$  (*bottom*).

used the Intel compilers and the Intel MKL library v2018.2, StarPU revision 581387c from the public GIT repository<sup>1</sup> and `qr_mumps` revision 2667<sup>2</sup>.

For these experiments, we have set the block size to  $m = 640$ ,  $n = 320$  and number of block-columns and block-rows  $c = 4094$ ; note that choosing  $c = 2^t - 2$  for some  $t$  ensures that when nested dissection is applied all the chains have the same length  $2^{t-l} - 2 \forall l = 1, \dots, t - 1$ . We will comment on how the behavior will change for different values of these parameters but we will not report further experiments because they do not provide additional insight to the experimental analysis. Two different tile sizes have been chosen for the partitioning of blocks within the `qr_mumps` operations, namely,  $b = 160$  and  $b = 320$ . Finally, we have executed experiments for varying values of the number of nested dissection levels  $l$  from 0 (i.e., no matrix permutation) to 5; going beyond this value does not make sense in our experimental setting because of the limited number of cores.

Table 3 shows the execution time of the  $QR$  factorization for different numbers of threads and values of the  $l$  parameter with  $b = 160$  in the top part and  $b = 320$  in the bottom part. The “-” entries correspond to the cases where the number of threads is lower than the number of chains  $2^l$ ; these are uninteresting because of the excessive flops overhead spent for an unnecessary amount of parallelism. When nested dissection is not used, scalability is obviously limited by the lack of parallelism; obviously, better results are obtained by using small tiles because higher parallelism is available within each branch of the tree. When

<sup>1</sup><https://gforge.inria.fr/projects/starpu/>

<sup>2</sup>[http://buttari.perso.enseiht.fr/qr\\_mumps/releases/qr\\_mumps\\_r2667.tgz](http://buttari.perso.enseiht.fr/qr_mumps/releases/qr_mumps_r2667.tgz)

		$l$					
		0	1	2	3	4	5
#threads	1	30.8	-	-	-	-	-
	2	60.0	60.9	-	-	-	-
	4	117.0	121.2	128.0	-	-	-
	8	180.0	234.2	249.5	251.5	-	-
	16	183.3	311.5	435.2	444.0	441.2	-
	32	182.5	303.1	590.8	600.7	615.8	603.1
	36	178.5	272.6	509.7	579.2	588.1	591.6
#threads	1	31.7	-	-	-	-	-
	2	57.8	63.8	-	-	-	-
	4	79.6	116.3	132.6	-	-	-
	8	90.1	158.5	268.8	268.5	-	-
	16	88.9	164.8	442.3	486.0	488.0	-
	32	82.6	165.0	482.5	901.9	932.0	907.4
	36	70.5	136.5	464.1	905.2	997.8	997.8

Table 4: Speed in Gflop/s for the  $QR$  factorization of a problem with  $m = 640$ ,  $n = 320$  and  $c = 4094$  with tile size  $b = 160$  (*top*) and  $b = 320$  (*bottom*).

one level of nested dissection is applied, parallelism is roughly doubled with no additional cost, which explains why the execution times in the second column of the table are always below the corresponding ones in the first. The improvement is, as expected, higher in the case of large tiles and when the number of threads grows. For values of  $l$  greater than or equal to two, the use of nested dissection implies a computational overhead. This explains why, when the number of threads is relatively low, increasing  $l$  results in a slowdown; this is especially true when small tiles are used because sufficient parallelism is available even with small values of  $l$ . When the number of threads is relatively high, the benefit of the additional parallelism overcomes the extra computational cost and the execution time is reduced. Additionally, we can observe that, when the number of threads is relatively high, the best results are achieved with large tiles: this is because of the larger granularity of tasks which allows for a better efficiency of the BLAS operations executed on tiles. Ultimately, we can conclude that, when the number of threads is relatively low, using small tiles and few levels of nested dissection provides sufficient parallelism with no or little computational overhead; inversely, when more threads are used, using large tiles is beneficial for improving the efficiency of elementary operations and the extra parallelism is worth the computational overhead. This is illustrated in Figure 7 (*left*) where the best execution times are taken along each row of Table 3 and compared to the best sequential result, i.e., 149.1s. The number next to each data point shows the nested dissection levels used to obtain the corresponding result. The best time improvement with respect to the sequential case is 15.8 for the case  $l = 4$  which results in roughly twice as many floating-point operations.

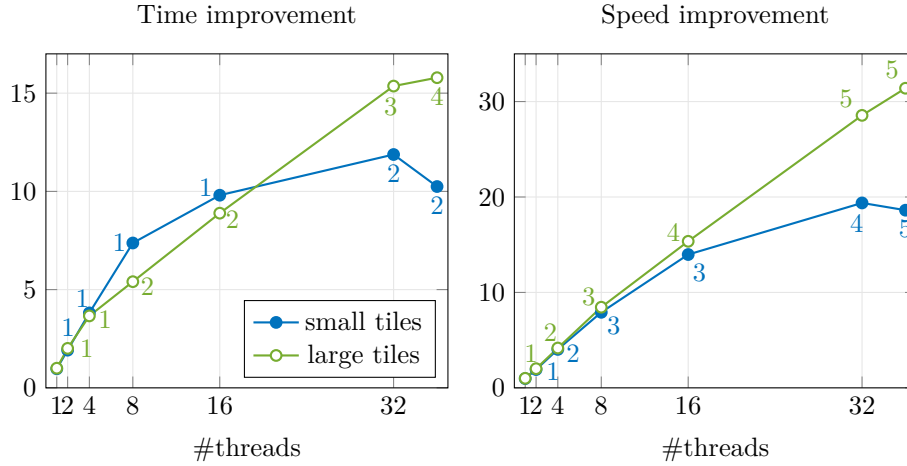


Figure 7: Best time and speed improvement over the sequential case. The values beside each data point shows the corresponding value of  $l$ .

	0	1	2	3	4	5
160	76.3	56.5	79.9	96.8	104.2	106.6
320	138.2	75.1	49.8	58.2	61.9	64.7
160	496.4	670.4	741.9	723.2	723.0	732.2
320	274.2	504.5	1191.3	1202.9	1217.1	1205.2

Table 5: Execution time (*top*) and speed in Gflop/s (*bottom*) for the  $QR$  factorization of a problem with  $m = 1280$ ,  $n = 640$  and  $c = 4094$  with tile size  $b = 160$  (*top*) and  $b = 320$  (*bottom*) on 36 cores.

In order to assess the efficiency and scalability of our implementation, in Table 4 we provide the speed of computations in Gigaflops per second which is insensitive to the computational overhead imposed by the use of nested dissection. As expected, performance grows for higher values of  $l$  because more embarrassing parallelism is available; for a given value of  $l$ , performance at first grows with the number of threads and eventually decreases when the available parallelism is not enough to feed all the working threads. The peak performance of a single core is 73.6 Gflop/s, which means that the sequential execution has an efficiency of 43%. This relatively poor efficiency can be explained by the relatively small values of  $m$  and  $n$  which makes the relative cost of BLAS-2 rich operations (i.e., `geqrt` and `tpqrt`) greater; higher speeds can be observed when larger blocks are used. The best speed improvement is a remarkable 31.4 out of 36; it must be noted that for the case of  $l = 5$ , roughly 99% of the computations are done in chain or leaf nodes.

For the sake of completeness, in Table 5 we report the execution time and

speed for the factorization of a matrix with large blocks ( $m = 1280$  and  $n = 640$ ) obtained with 36 threads. In this case, more parallelism is available within each branch and, consequently, the best shortest execution time is achieved with fewer levels of nested dissection with respect to the previous case. It can also be noted that the overall performance is higher thanks to a better ratio between Level-3 and Level-2 BLAS operations; this also holds for the sequential case where the execution time is 960.7 seconds for a speed of 39.46 Gflop/s.

Although, as discussed above, some concurrency is available within each branch or node of the tree, this parallelism involves communications due to the fact that multiple processes share the same data. On shared memory systems, these communications take the form of memory traffic and synchronizations. In distributed memory systems, these communications amount to transferring data through the slow network interconnection and, therefore, are much more penalizing. The use of nested dissection introduces embarrassing parallelism because each process may potentially work on a different branch without communicating with others. For this reason, we speculate that the benefit of increasing  $l$  over the operational overhead is better on distributed memory systems than shared memory ones. We reserve the development and analysis of a distributed memory parallel implementation for the future.

## 5 Conclusion

In this work, we have presented a method for computing the  $QR$  factorization of block-tridiagonal matrices. Our approach draws parallelism from the nested dissection method which allows for structuring the elimination process as a parallel topological order traversal of a tree graph. At each node of this tree, one block-column is reduced through Householder reflections. These operations are computed in such a way that the sparsity of the data handled at each node of the tree is taken advantage of.

A detailed analysis of the operational and memory complexity of the resulting method was provided. Although we demonstrated that this complexity grows with the number of used nested dissection levels, the overhead with respect to the sequential (i.e., no nested dissection) case is bounded by a moderate constant.

An actual implementation of the factorization method that can take advantage of multiple levels of parallelism was also presented. Not only does our solver achieve parallelism through the concurrent traversal of separate branches of the elimination tree but also from the intrinsic concurrency available at each tree node and from pipelining the processing of nodes at different levels of the tree. This is achieved by using the parallel, asynchronous dense linear algebra methods available in the `qr_mumps` software and developing the missing operations.

Finally, experimental results on a shared memory architecture that show the effectiveness of our approach as well as of its actual implementation were included.

## 6 Acknowledgments

This work was granted access to the HPC resources of CALMIP supercomputing center under the allocation 2018-p0989. S. Hauberg was supported by a research grant (15334) from VILLUM FONDEN. C. Kodsı and S. Hauberg have received funding from the European Research Council (ERC) under the European Union’s Horizon 2020 research and innovation programme (grant agreement n° 757360).

## References

- [1] Patrick R. Amestoy, Iain S. Duff, and Chiara Puglisi. “Multifrontal QR factorization in a multiprocessor environment”. In: *Int. Journal of Num. Linear Alg. and Appl.* 3(4) (1996), pp. 275–300. DOI: [10.1002/\(SICI\)1099-1506\(199607/08\)3:4<275::AID-NLA83>3.0.CO;2-7](https://doi.org/10.1002/(SICI)1099-1506(199607/08)3:4<275::AID-NLA83>3.0.CO;2-7).
- [2] Peter Arbenz and Markus Hegland. “On the stable parallel solution of general narrow banded linear systems”. In: *High performance algorithms for structured matrix problems*. Vol. 2. Adv. Theory Comput. Math. Commack, NY: Nova Sci. Publ., 1998, pp. 47–73.
- [3] Georgios Arvanitidis, Lars Kai Hansen, and Søren Hauberg. “Latent Space Oddity: on the Curvature of Deep Generative Models”. In: *International Conference on Learning Representations (ICLR)*. 2018.
- [4] Cedric Augonnet et al. “StarPU: A Unified Platform for Task Scheduling on Heterogeneous Multicore Architectures”. In: *Concurrency and Computation: Practice and Experience, Special Issue: Euro-Par 2009 23* (2 Feb. 2011), pp. 187–198. DOI: [10.1002/cpe.1631](https://doi.org/10.1002/cpe.1631).
- [5] Yoshua Bengio, Aaron Courville, and Pascal Vincent. “Representation learning: A review and new perspectives”. In: *IEEE transactions on pattern analysis and machine intelligence* 35.8 (2013), pp. 1798–1828.
- [6] Michael W. Berry and Ahmed Sameh. “Multiprocessor Schemes for Solving Block Tridiagonal Linear Systems”. In: *The International Journal of Supercomputing Applications* 2.3 (1988), pp. 37–57. DOI: [10.1177/109434208800200304](https://doi.org/10.1177/109434208800200304).
- [7] Henricus Bouwmeester et al. “Tiled QR Factorization Algorithms”. In: *Proceedings of 2011 International Conference for High Performance Computing, Networking, Storage and Analysis*. SC ’11. Seattle, Washington: ACM, 2011, 7:1–7:11. ISBN: 978-1-4503-0771-0. DOI: [10.1145/2063384.2063393](https://doi.org/10.1145/2063384.2063393).
- [8] Alfredo Buttari. “Fine-Grained Multithreading for the Multifrontal QR Factorization of Sparse Matrices”. In: *SIAM Journal on Scientific Computing* 35.4 (2013), pp. C323–C345. DOI: [10.1137/110846427](https://doi.org/10.1137/110846427).

- [9] Alfredo Buttari et al. “A class of parallel tiled linear algebra algorithms for multicore architectures”. In: *Parallel Comput.* 35 (1 Jan. 2009), pp. 38–53. ISSN: 0167-8191. DOI: [10.1016/j.parco.2008.10.002](https://doi.org/10.1016/j.parco.2008.10.002).
- [10] Tim Davis. *Direct Methods for Sparse Linear Systems*. Society for Industrial and Applied Mathematics, 2006. DOI: [10.1137/1.9780898718881](https://doi.org/10.1137/1.9780898718881).
- [11] Timothy A. Davis. “Algorithm 915, SuiteSparseQR: Multifrontal multi-threaded rank-revealing sparse QR factorization”. In: *ACM Trans. Math. Softw.* 38.1 (Dec. 2011), 8:1–8:22. ISSN: 0098-3500. DOI: [10.1145/2049662.2049670](https://doi.org/10.1145/2049662.2049670).
- [12] James Demmel et al. “Communication-optimal Parallel and Sequential QR and LU Factorizations”. In: *SIAM J. Sci. Comput.* 34.1 (Feb. 2012), pp. 206–239. ISSN: 1064-8275. URL: <http://dx.doi.org/10.1137/080731992>.
- [13] Iain S Duff, Albert M Erisman, and John K Reid. *Direct Methods for Sparse Matrices*. New York, NY, USA: Oxford University Press, Inc., 1986. ISBN: 0-198-53408-6.
- [14] W. Morven Gentleman. “Row elimination for solving sparse linear systems and least squares problems”. In: *Numerical Analysis*. Ed. by G. Alistair Watson. Berlin, Heidelberg: Springer Berlin Heidelberg, 1976, pp. 122–133. ISBN: 978-3-540-38129-7. DOI: [10.1007/BFb0080119](https://doi.org/10.1007/BFb0080119).
- [15] Alan J. George. “Nested dissection of a regular finite-element mesh”. In: *SIAM J. Numer. Anal.* 10.2 (1973), pp. 345–363. DOI: [10.1137/0710032](https://doi.org/10.1137/0710032).
- [16] Søren Hauberg. “Only Bayes should learn a manifold”. In: (2018).
- [17] Markus Hegland. “On the parallel solution of tridiagonal systems by wrap-around partitioning and incomplete LU factorization”. In: *Numerische Mathematik* 59.1 (Dec. 1991), pp. 453–472. ISSN: 0945-3245. DOI: [10.1007/BF01385791](https://doi.org/10.1007/BF01385791).
- [18] Markus Hegland and Mike Osborne. “Algorithms for Block Bidiagonal Systems on Vector and Parallel Computers”. In: *Proceedings of the 12th International Conference on Supercomputing*. ICS ’98. Melbourne, Australia: ACM, 1998, pp. 1–6. ISBN: 0-89791-998-X. DOI: [10.1145/277830.277835](https://doi.org/10.1145/277830.277835).
- [19] R. W. Hockney. “A Fast Direct Solution of Poisson’s Equation Using Fourier Analysis”. In: *J. ACM* 12.1 (Jan. 1965), pp. 95–113. ISSN: 0004-5411. DOI: [10.1145/321250.321259](https://doi.org/10.1145/321250.321259).
- [20] Jospeh W. H. Liu. “The Role of Elimination Trees in Sparse Factorization”. In: *SIAM Journal on Matrix Analysis and Applications* 11 (1990), pp. 134–172. DOI: [10.1137/0611010](https://doi.org/10.1137/0611010).
- [21] Eric Polizzi and Ahmed H. Sameh. “A parallel hybrid banded system solver: the SPIKE algorithm”. In: *Parallel Computing* 32.2 (2006). Parallel Matrix Algorithms and Applications (PMAA’04), pp. 177–194. ISSN: 0167-8191. DOI: <https://doi.org/10.1016/j.parco.2005.07.005>.

- [22] Donald J. Rose, R. Endre Tarjan, and George S. Lueker. “Algorithmic Aspects of Vertex Elimination on Graphs”. In: *SIAM Journal on Computing* 5.2 (1976), pp. 266–283. DOI: [10.1137/0205021](https://doi.org/10.1137/0205021).
- [23] A. Sameh. “On Two Numerical Algorithms for Multiprocessors”. In: *Proc. of NATO Adv. Res. Workshop on High-Speed Comp., Series F: Computer and Systems Sciences*. Vol. 7. 1984, pp. 311–328.
- [24] A. H. Sameh and D. J. Kuck. “On Stable Parallel Linear System Solvers”. In: *J. ACM* 25.1 (Jan. 1978), pp. 81–91. ISSN: 0004-5411. DOI: [10.1145/322047.322054](https://doi.org/10.1145/322047.322054).

## A Pivotal sequences

**Leaf nodes** The matrix blocks concerned by the operations on a leaf node are depicted in Figure 8 (*left*). At leaf node  $k$ , these are in columns  $k, k + 1, k + 2, a_1, a_2$  and rows  $k, k + 1, a_1$  where  $a_1$  and  $a_2$  are block-columns associated with an ancestor separator, the one that the chain is moving away from. Because the two outer branches are not moving away from any separator, only the first three rows and columns are concerned by the processing of a leaf node attached to one such chain, as illustrated by the dashed green line in the figure. The operations executed on a leaf node result in the structure shown in the right part of the figure and are described by the following pivotal sequence:

$$\begin{aligned}
& GE(B_{k,k}^7), GE(B_{k+1,k}^7), TP(B_{k,k}^1, B_{k+1,k}^1), GE(B_{a_1,k}^7), \\
& TP(B_{k,k}^1, B_{a_1,k}^1), GE(B_{k+1,k+1}^7), TP(B_{k+1,k+1}^1, B_{k,k+1}^6), \\
& TP(B_{k+1,k+1}^1, B_{a_1,k+1}^1), GE(B_{k+1,k+2}^6), TP(B_{k+1,k+2}^2, B_{k,k+2}^6), \\
& TP(B_{k+1,k+2}^2, B_{a_1,k+2}^1), GE(B_{a_1,a_1}^7), GE(B_{a_1,a_2}^6), \\
& TP(B_{a_1,a_1}^1, B_{k,a_1}^6), TP(B_{a_1,a_1}^1, B_{k+1,a_1}^4), \\
& TP(B_{a_1,a_2}^2, B_{k,a_2}^6), TP(B_{a_1,a_2}^2, B_{k+1,a_2}^4).
\end{aligned}$$

Operations that involve blocks in row or column  $a_1$  or  $a_2$  need not be executed for leaf nodes attached to outer branches. As a reminder of what was said in Section 2, at the end of these operations the  $k$ -th block-row of the global  $R$  factor is computed, highlighted in red in Figure 8 (*right*); the blue blocks will be operated upon in nodes along the branch connecting the leaf to the root of the tree while the gray blocks correspond to the Householder vectors that implicitly represent the  $Q$  factor.

**Separator nodes** The blocks concerned by the operations on a separator node are depicted in Figure 9 (*left*). When all the chain nodes have been eliminated, each separator (except the two outer ones) is connected to two other separators: one is the parent node and the other an ancestor node in the tree. Therefore, these blocks are in columns  $s_1, s_2, p_1, p_2, a_1, a_2$  and rows  $s_1, s_2, p_1, a_1,$

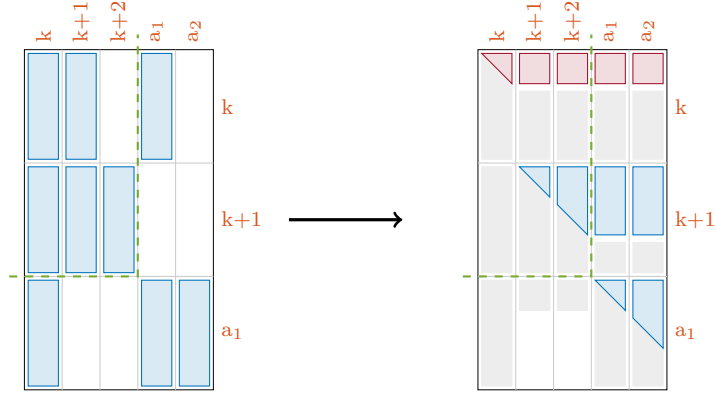


Figure 8: The blocks concerned by the operations at leaf node  $k$ . Their structure before and after the processing of the node are shown in the left and right parts of the figure, respectively. The green dashed line shows the difference between inner and outer leaf nodes.

where  $s_1$  and  $s_2$  are the block-columns associated with the separator,  $p_1$  and  $p_2$  those associated with the parent separator and  $a_1, a_2$  those associated with the ancestor separator. Separators belonging to one of the two outer branches are only connected to their parent and, therefore, columns  $a_1, a_2$  and row  $a_1$  do not exist; this is illustrated by the dashed green line in Figure 9. Finally, the root node is a separator which does not have a parent nor an ancestor and, therefore, only the first two rows and columns are involved in its processing, as illustrated by the dashed purple line in Figure 9. The operations executed on a separator node result in the structure shown in the right part of the figure and are described by the following pivotal sequence:

$$\begin{aligned}
& TP(B_{s_1, s_1}^1, B_{s_2, s_1}^1), \quad GE(B_{s_2, s_2}^1), \quad TP(B_{s_2, s_2}^1, B_{s_1, s_2}^2), \quad TP(B_{s_2, s_2}^1, B_{s_2, s_2}^2), \\
& TP(B_{p_1, p_1}^1, B_{s_1, p_1}^2), \quad TP(B_{p_1, p_1}^1, B_{s_2, p_1}^2), \\
& TP(B_{p_1, p_2}^2, B_{s_1, p_2}^2), \quad TP(B_{p_1, p_2}^2, B_{s_2, p_2}^2), \\
& TP(B_{a_1, a_1}^1, B_{s_1, a_1}^2), \quad TP(B_{a_1, a_1}^1, B_{s_2, a_1}^2), \\
& TP(B_{a_1, a_2}^2, B_{s_1, a_2}^2), \quad TP(B_{a_1, a_2}^2, B_{s_2, a_2}^2).
\end{aligned}$$

All the operations involving rows and columns  $a_1$  and  $a_2$  need not be done on outer separators and the root; all those involving rows and columns  $p_1$  and  $p_2$  need not be done on the root.



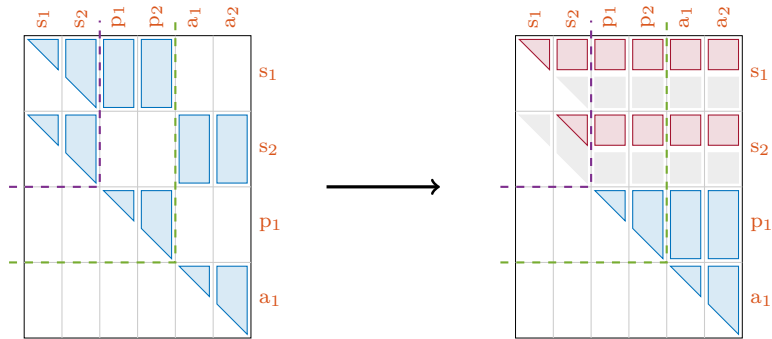


Figure 9: The blocks concerned by the operations at separator node  $(s_1, s_2)$ . Their structure before and after the processing of the node are shown in the left and right parts of the figure, respectively. The green dashed line shows the difference between inner and outer separator nodes. The purple dashed line delimits the rows and columns of the tree root node.